NeuroImage 125 (2016) 144–152

Contents lists available at ScienceDirect

NeuroImage

journal homepage: www.elsevier.com/locate/ynimg

Morphological maturation of the mouse brain: An in vivo MRI and histology investigation

Luam Hammelrath [a], Siniša Škokić [a,b], Artem Khmelinskii [c,d], Andreas Hess [e], Noortje van der Knaap [a,f], Marius Staring [c], Boudewijn P.F. Lelieveldt [c,g], Dirk Wiedermann [a], Mathias Hoehn [a,c,d,*]

[a] Max Planck Institute for Metabolism Research, In-vivo-NMR Laboratory, Gleuelerstraße 50, Cologne, Germany
[b] Croatian Institute for Brain Research, University of Zagreb School of Medicine, Šalata 12, Zagreb 10000, Croatia
[c] Division of Image Processing, Dept. of Radiology, Leiden University Medical Center, PO Box 9600, 2300 RC Leiden, The Netherlands
[d] Percuros B.V., Drienerlolaan 5-Zuidhorst, 7522 Enschede, NB, The Netherlands
[e] Institute of Experimental and Clinical Pharmacology and Toxicology, University of Erlangen-Nürnberg, Fahrstr. 17, 91054 Erlangen, Germany
[f] Donders Institute for Brain, Cognition and Behaviour, Dept. of Cognitive Neuroscience, Radboud University Nijmegen, P.O. Box 9010, 6500 GL Nijmegen, The Netherlands
[g] Dept. of Intelligent Systems, Delft University of Technology, Mekelweg 4, 2628 CD Delft, The Netherlands

ARTICLE INFO

Article history:
Received 31 July 2015
Accepted 5 October 2015
Available online 14 October 2015

Keywords:
MRI
Mouse brain
Brain development
Cortex
Myelination
DTI

ABSTRACT

With the wide access to studies of selected gene expressions in transgenic animals, mice have become the dominant species as cerebral disease models. Many of these studies are performed on animals of not more than eight weeks, declared as adult animals. Based on the earlier reports that full brain maturation requires at least three months in rats, there is a clear need to discern the corresponding minimal animal age to provide an "adult brain" in mice in order to avoid modulation of disease progression/therapy studies by ongoing developmental changes. For this purpose, we have studied anatomical brain alterations of mice during their first six months of age. Using T2-weighted and diffusion-weighted MRI, structural and volume changes of the brain were identified and compared with histological analysis of myelination. Mouse brain volume was found to be almost stable already at three weeks, but cortex thickness kept decreasing continuously with maximal changes during the first three months. Myelination is still increasing between three and six months, although most dramatic changes are over by three months. While our results emphasize that mice should be at least three months old when adult animals are needed for brain studies, preferred choice of one particular metric for future investigation goals will result in somewhat varying age windows of stabilization.

Introduction

The development of the brain continues well beyond birth and goes through various phases of adolescent changes (Andersen, 2003; Meaney and Stewart, 1981; Spear and Brake, 1983) before it reaches a state in adulthood which is considered a steady state condition. Such steady state is usually assumed when adult animals are studied, be it in the course of neurodevelopmental studies (Tissir and Goffinet, 2003) or for the investigation into cerebral disease evolutions (Adamczak et al., 2014; van Dorsten et al., 1999) and development of corresponding therapeutic strategies (Bockhorst et al., 2008). This requires the definition of a time window in early age when this cerebral maturation has been reached as well as the definition of a time window in progressed age when aging processes start to disturb this steady state. The definition of the onset of adulthood and the end of maturation is the goal of the present study. Often, adulthood of experimental animals was used equivalent to full sexual maturity or to body weight indications only. However, in an earlier study on rat brain maturation we have been able to point out a wide temporal discrepancy of sexual maturity to full brain maturation (Mengler et al., 2014).

With the wide access to studies of selected gene expressions in transgenic animals, mice have become the dominant species for experimental investigations on cerebral diseases, including stroke (Adamczak et al., 2014), neurodegenerative diseases such as Alzheimer's disease (Zempel and Mandelkow, 2014), trauma (Webster et al., 2015) and many more. Many of these studies are performed on animals of not more than eight weeks, declared as adult animals. Based on the earlier reported situation on rats that full brain maturation requires animals with an age of at least three months (Mengler et al., 2014), there is a clear need to discern

* Corresponding author at: In-vivo-NMR Laboratory, Max Planck Institute for Metabolism Research, Gleuelerstrasse 50, D-50931 Köln, Germany.
E-mail addresses: Luam.Mengler@sf.mpg.de (L. Hammelrath), sskokic@hiim.hr (S. Škokić), A.Khmelinskii@lumc.nl (A. Khmelinskii), andreas.hess@fau.de (A. Hess), Noortje.vanderKnaap@radboudumc.nl (N. van der Knaap), M.Staring@lumc.nl (M. Staring), B.P.F.Lelieveldt@lumc.nl (B.P.F. Lelieveldt), dirk.wiedermann@sf.mpg.de (D. Wiedermann), mathias@sf.mpg.de (M. Hoehn).

http://dx.doi.org/10.1016/j.neuroimage.2015.10.009

the corresponding minimal animal age to provide an "adult brain" in mice.

Magnetic resonance imaging (MRI) has become an indispensible tool in neuroanatomy. MRI provides information on macrostructural as well as microstructural changes in the intact tissue, without suffering from shrinkage or other preparation artifacts, like shearing or cutting artifacts. The non-invasive character of MRI allows a longitudinal investigation of subjects and can complement histology when studying development, aging or disease models. Especially in postnatal development, MRI has proven useful for the detection and measurement of region specific growth and myelination (Wozniak and Lim, 2006). The relative water content of a tissue contributes greatly to contrast based on the spin–spin relaxation time contrast T2. Additionally, the different water diffusion characteristics in tissues are captured in diffusion tensor imaging (DTI); the structural complexity of a tissue not only changes the degree of diffusion, but also the directionality of the water movement. In recent years, postnatal development in rodent brains was frequently studied using DTI of ex vivo specimen (Mori et al., 2001; Zhang et al., 2003, 2005). These studies have built a fair basis for DTI-based morphometry of white matter. However, they lack detailed gray matter characterization and only few studies were performed with true in vivo measurements.

Neurodevelopmental studies of cerebral and in particular of cortical morphology can help identify structural, anatomic changes and reorganizations. Here, we have employed T2 relaxivity and DTI MRI in order to visualize microscopic as well as morphometric changes of the mouse brain and to unravel the time profile of the development and maturation of cortical structures.

Methods

Animals

All experiments were performed on C57Bl/6J mice (Janvier, Le Genest Saint Isle, Cedex, France) of four different postnatal ages: three, eight, twelve and twenty-four weeks.

Animals were allowed two weeks of habituation upon arrival. Weaning mice (P21) were born in the facility. They were housed in groups of four and were given access to food and water ad libitum, in an environment with controlled temperature (21 +/− 1 °C), humidity (55 +/− 10%), and light (12/12 h dark/light cycle). All animal experiments were conducted in accordance with the German Animal Welfare Act and approved by the local authorities (Landesamt für Naturschutz, Umwelt und Verbraucherschutz NRW).

MRI acquisition and data processing

MRI experiments were conducted on a 9.4 T Bruker BioSpec horizontal bore, dedicated animal scanner (Bruker Biospin, Ettlingen, Germany), equipped with a gradient system of 660 mT/m at 110 μs ramp time. For RF excitation a quadrature volume resonator (inner diameter 72 mm; Bruker Biospin) was used, for signal reception a quadrature mouse brain surface coil (Bruker Biospin) was applied. MRI data was acquired using Paravision 5.1 software. After induction of anesthesia, mice were placed in an MRI compatible cradle (Bruker Biospin), and the head was fixed with ear bars and a support ring for the upper incisors in order to reduce movement artifacts. Animals were anesthetized with 2% isoflurane (Forane, Baxter, Deerfield, IL, USA) in a 70/30 mixture of N_20 and O_2; vital functions were monitored during the whole anesthesia period using DASYLab (version 9.0, Measurement Computing Cooperation, Norton, MA, USA). The breathing rate was assessed via a breathing pillow, placed under the thorax, and kept at 100–120 breaths/min by adjusting the isoflurane concentration. Body temperature was recorded with a rectal temperature probe, and regulated by adjusting the temperature of a warm water circulation system (Medres, Cologne, Germany), feeding a heating blanket and the MR cradle.

T2WI and DTI protocols were set to cover the volume between the rhinal fissure and the anterior part of the cerebellum, and imaging data was acquired with identical geometry for both scans (field of view: 28 mm × 28 mm, matrix 192 × 192, 0.5 mm slice thickness, no inter-slice gaps). The number of slices was adjusted individually in every session according to age dependent brain size.

T2W images were acquired with a multi slice multi echo sequence (MSME TR/TE = 5000 ms/10 ms; 10 echoes, with 10 ms inter-echo spacing). For every voxel a monoexponential decay curve was determined from the ten echoes of the MSME (IDL version 6.4, Boulder, CO, USA) and the resulting spin–spin relaxation time was calculated pixelwise to obtain quantitative T2 maps.

Diffusion tensor imaging was recorded with an 8-shot spin echo EPI sequence (30 directions; b-value = 670 s/mm^2, and five supplementary A0 images), with a gradient scheme according to Jones 30 (Jones et al., 1999; Skare et al., 2000). DTI data is prone to distortions due to eddy currents, induced when strong gradient pulses are switched on and off, and to motion artifacts originating from the subject. Prior to tensor calculation, we therefore applied an eddy current correction (FSL version 4.1.7, FMRIB Centre, Oxford, UK) and visually inspected the single frames, discarding the corrupted ones. The occurrence of other distortions and artifacts was limited during image acquisition by applying an automatic ghost correction, the use of a fat suppression module (1.9 ms Gaussian pulse, 1,400 Hz bandwidth, 2 ms spoiler) and navigator echoes. The total acquisition time added up to 50 min, including adjustment scans and a full brain RARE sequence. The RARE data set was used for co-registration of measurements at separate time points.

From the diffusion tensor, three eigenvectors and the corresponding eigenvalues (λ_1, λ_2, λ_3) can be determined, representing in each voxel the main diffusion directions and the magnitude of diffusivity in all three directions. The largest eigenvalue (λ_1) represents the axial or parallel diffusivity ($\lambda_\parallel$), while the perpendicular or radial diffusivity ($\lambda_\perp$) is the average of the two minor values, the second (λ_2) and third eigenvalue (λ_3). The average of all three eigenvalues is a measure for the mean diffusivity (MD) (Basser et al., 1994). Based on the three eigenvalues, the fractional anisotropy (FA) is calculated, giving a measure for the anisotropy of diffusion within the voxel ($0 < FA < 1$, where 0 = isotropic condition).

Registration procedure and deformation-based morphometry (DBM)

The first echo of the MSME yields the best anatomical contrast and a high SNR, thus best qualifying for co-registration of individual image data sets. The images were stripped of external tissue (Smith, 2002) and normalized to a template brain compiled of n = 24 nine week old C57/Bl6 mice. The registration followed a hierarchical scheme (Mengler et al., 2014) and was implemented using Elastix (Klein et al., 2010). Detailed information on registration parameters can be found here (http://elastix.bigr.nl/wiki/index.php/Par0025). Two independent raters controlled the quality and success of the registration process using a custom-made graphic user-interface (Khmelinskii et al., 2013). Subsequently, the displacement field, containing the local deformations relative to the template, was applied to re-orient the calculated maps derived from the T2WI and DTI datasets.

The template was manually labeled with anatomical brain regions of interest (see below), and the corresponding volumes of interests (VOIs) were mapped in the native space of the individual datasets.

The displacement field encodes the anatomical differences between two ages of a brain, such that each voxel describes the transformation vector to the homologous position. A measure derived from the deformation matrix is the determinant of the Jacobian (detJac), representing the local volumetric changes. The detJac ranges from 0 (100% shrinkage) over 1 (no volume change) without upper boundary (volume increase). A logarithmic transform makes the Jacobian distribution symmetric, setting aside every a priori assumption on volume growth (Leow et al., 2006; Yanovsky et al., 2008). Volume changes were evaluated based

on this log detJac using MATLAB 2011b (MathWorks Inc., Natick, MA, USA).

ROI analysis

Quantitative MRI parameters were evaluated for specific regions focussing on key structures, both in white and gray matter. Gray matter structures were manually segmented within the template brain, covering the cerebral cortex, thalamus, hippocampus and striatum (Inline Supplementary Fig. S1). The corresponding regions of interest (ROIs) were transformed to the individual datasets, using the inverse displacement fields generated during the registration process, and evaluated for volume of the tissue structure and its quantitative MRI parameters. As white matter structures are rather small, their boundaries are blurred on MRI data, due to partial volume effects, making transformation delicate. In order to avoid transformation errors, particularly when adjusting for local tissue expansion and brain growth, ROIs were created on averaged age maps generated of the respective age group data, acting as age-specific "templates". The following white matter structures were analyzed: corpus callosum, fimbrium, external and internal capsule.

Inline Supplementary Fig. S1 can be found online at http://dx.doi.org/10.1016/j.neuroimage.2015.10.009.

Using the same strategy, the cortex was segmented into cortical layers (upper, middle and lower cortex) on the first echo image of the multi-echo spin echo sequence. This was executed for different cortex areas: motor cortex (M1), primary somatosensory cortex of the forelimbs (S1), whisker barrel field of the somatosensory cortex (BF) and secondary somatosensory cortex (S2).

Cortical thickness determination

Cortical thickness measurements were performed on the individual datasets as well as on the age group average datasets. For the former the original MRI datasets per age were affine registered. In all cases the cortex was manually segmented. This resulted in a surface representation of the cortex with outer and inner boundaries. For each surface element (triangle) of the cortical outer boundary the surface normal was calculated. This surface normal is perpendicular to the surface therefore running from the outer to the inner boundary of the cortex. The length of this surface normal from the outer to the inner boundaries corresponds to the thickness of the cortex at that position. The thickness and position for every surface element were stored in a so called surface lattice. This surface lattice was mapped onto the outer cortex and color coded (cf. Fig. 3)

Next, in order to determine the most anterior and posterior coordinates for M1 and S1 a 3D mouse brain atlas, derived from Franklin & Paxinos (Franklin, 2007) was affine registered to every dataset. From the most anterior to the most posterior landmark for M1 and S1 a path was interpolated along the outer cortex surface. Additionally, a supplementary path along the lateral aspect of the cortex was created, stretching from the most anterior to the most posterior part of the segmented cortex. The cortical thickness at each coordinate of the different paths was obtained as the thickness value from the nearest element of the surface lattice.

From the individual datasets of these thickness profiles (Inline Supplementary Fig. S3) the averaged values across all animals of a given age are also presented (cf. Fig. 3).

Inline Supplementary Fig. S3 can be found online at http://dx.doi.org/10.1016/j.neuroimage.2015.10.009.

Histological examination

After the MRI session, mice were deeply anesthetized with isoflurane and perfused transcardially with saline, followed by 4% PFA. Brains were extracted, postfixed overnight and kept in sucrose solution until they sank. Specimens were serially sectioned at 30 μm on a freezing microtome (Leica Microsystems, Wetzlar, Germany) and kept at −20 °C in cryo-protective solution. After mounting on glass slides, sections were washed, heated, and stained for myelin before dehydrating in alcohol, clearing, and coverslipping. Myelin staining was achieved with the black-gold technique (Schmued et al., 2008) until fine fibers of the molecular layer appeared in the 24 week specimen. At selected levels, overview images of the sections were taken with 4× magnification (Keyence BZ-9000, Keyence Corp., Neu-Isenburg, Germany). ROIs in the upper, central and lower part of the S1 and M1 were chosen and corresponding images acquired with 40× magnification. ROI images were transformed into binary images using the "make binary" tool implemented into ImageJ software (version 1.46r, NIH, Bethesda, MD, USA) without applying supplementary thresholds. Black areas were defined as "stained for myelin". All postprocessing and analysis was performed using ImageJ software.

Statistical analysis

As MRI parameters of the same subject cannot be considered independent data, MANOVAs for the different parameters were performed to find differences between the age groups. Significant MANOVAs were followed up by separate ANOVAs for the individual ROIs. A Tukey HSD test, for post hoc pair-wise comparisons, revealed differences within a variable and ROI and between ages (all in SPSS version 22, IBM Corp. Armonk, NY, USA).

Results

Tissue selective ROI analysis of MRI parameters during developmental changes

ROI-based analysis of the T2 relaxation time values showed an initial decrease of T2 both in white and in gray matter from three to eight weeks of age. From eight weeks on, the T2 values were increasing slightly and continuously, continuing even till 24 weeks of age (Fig. 1). Using Pillai's trace there was a detectable effect of age on T2 values ($V = 2.49$, $F(27, 18) = 3.275$, $p < 0.01$). Separate ANOVAs for the different ROIs supported this effect to be highly significant for every ROI, except for the fimbrium. Results of the post hoc pairwise comparisons (Tukey HSD test) between the ages are illustrated in Fig. 1.

The DTI derived parameters revealed a more differentiated time profile. Fractional anisotropy (FA) was increasing in all white matter structures, except the internal capsule (ic). In gray matter, FA values went through a maximum at eight weeks of age in the hippocampus and caudate putamen but there was no clear age pattern in the thalamus. In the cortex, the FA value was continuously decreasing from three weeks of age on (Fig. 1). According to Pillai's trace there was an effect of age on fractional anisotropy values ($V = 2.46, F(27, 15) = 2.53, p < 0.05$). However, separate univariate ANOVAs on the individual ROIs revealed significant effects for the FA in the external capsule only ($F(3,11) = 10.869$, $p \le 0.001$). This effect did not reach statistical relevance in the pairwise comparison. Corresponding behavior of axial diffusivity, proton density and of radial diffusivity did not show any significant effect of age in multivariate or univariate ANOVAs.

When analyzing volumes of defined tissue areas over time, it is noted that for all gray matter regions analyzed the final volume is reached within the first eight postnatal weeks, with no further global or local volume changes observable after this time point (Fig. 2A). A strong effect of age is supported by a multivariate ANOVA, $F(15, 51) = 4.843$, $p < 0.001$, post hoc pairwise comparison revealed that significant differences occur only until week eight. The volume increase, however, is not substantial enough to be clearly revealed in the deformation-based morphometry, showing mostly volume reduction

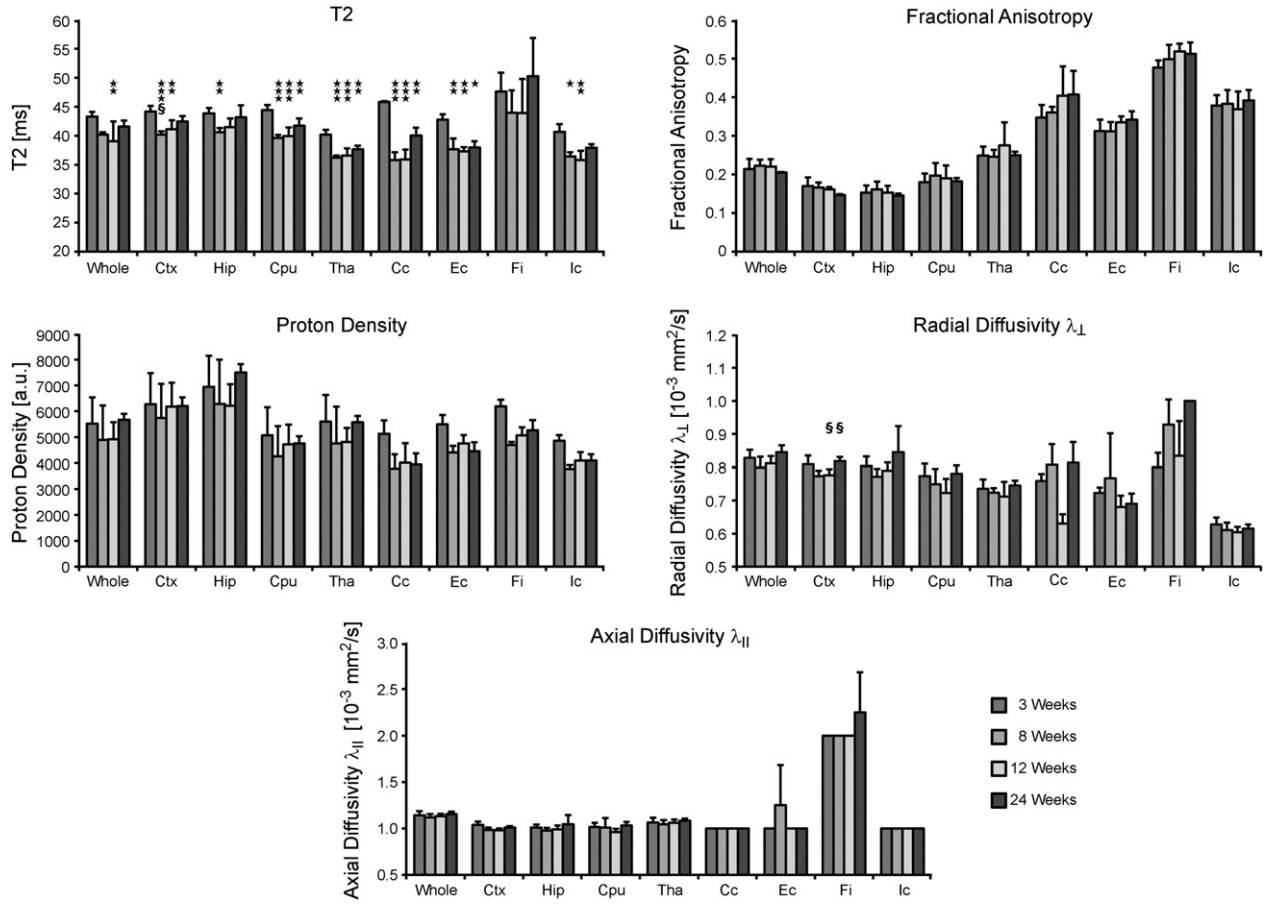

Fig. 1. Quantitative MRI parameters in different ROIs. The data shown is the group average of the different ages for T2, fractional anisotropy (FA), proton density, radial (RD) and axial diffusivity. Nine different ROIs in gray and white matter were analyzed: whole brain (whole), cortex (ctx), hippocampus (hip), striatum (Cpu), thalamus (Tha), corpus callosum (Cc), external capsule (Ec), fimbrium (Fi), internal capsule (Ic). The error bars indicate the standard error of the mean (SEM). Significance levels of post hoc pair-wise comparisons are indicated by the following symbols: significantly different from three weeks with $p < 0.05$ *; $p < 0.01$ **; $p < 0.001$ ***/significantly different from twelve weeks with $p < 0.05$ ♦; $p < 0.01$ ♦♦; $p < 0.001$ ♦♦♦/ significantly different from 24 weeks with $p < 0.05$ §; $p < 0.01$ §§; $p < 0.001$ §§§.

of ventricular cavities and only slight volume increases in the deep gray matter of the thalamus (Fig. 2B).

Age dependent changes in the cortex

The cortex thickness is decreasing from rostral to caudal direction. This pattern is preserved during all stages in the observation period (3–24 weeks) as depicted in the 3-dimensional color-coded cortex thickness maps in Fig. 3. The most caudal part (visual cortex) is thinnest while the rostro-medial cortex area around the motor cortex showed the largest thickness. Focusing on individual anatomical regions, their local absolute values also decrease with increasing age, indicating a continuing flattening of the cortex over time. This effect was found most pronounced in the most rostral end of the motor and somatosensory cortex regions, selected here for visualization (Fig. 3). As the whole brain still expands during the observation period, this cortical flattening largely counteracts the expected volume increase of the cortex.

T2- and DTI-derived contrast did not permit to discriminate the histologically defined cortical layer structure. Nevertheless, robust radial variation of fractional anisotropy contrast permitted a subdivision of the cortex into upper, central and lower cortical sections, as outlined in Fig. 4. Analysis of these three sections was performed for both FA and T2 parameters in the primary somatosensory cortex S1 and the motor cortex M1 as the anatomical regions of utmost interest (the results for S2 somatosensory cortex and barrel field cortex are presented in Inline Supplementary Fig. S2). A clear cortical depth dependent variation is observed for fractional anisotropy (Fig. 4 top diagrams), which was lost in the earlier analysis of the whole cortex as a single ROI (Fig. 1). This cortical depth dependent variation was noted irrespective of age within the first six months. The T2 values on the other hand did not reflect a section dependent variation (Fig. 4, bottom diagrams).

Inline Supplementary Fig. S2 can be found online at http://dx.doi.org/10.1016/j.neuroimage.2015.10.009.

Investigating T2 in the different cortical sections, using a multivariate ANOVA showed a significant effect of age in S1 and M1 ($V = 0.78$, $F(6,64) = 6.77$, $p < 0.001$). Post hoc pairwise comparisons (Tukey HSD) revealed highly significant differences between all age groups in the upper and central layers of M1 ($p < 0.01$) and between three weeks and the other ages in the lower layer. In S1, T2 was significantly decreasing after three weeks, followed by a gradual increase from eight weeks on. Despite this increase, T2 values did not reach the T2 values at weaning age at three weeks but stayed significantly below this three week value in the lower and central sections.

Fractional anisotropy (FA) seems to be more layer dependent than T2. While FA was decreasing in the upper and central layers over time, both in S1 and in M1, it remained unchanged in the lower layer for S1, but was even slightly increasing with age in M1. However, these observations did not reach statistical significance in a multivariate ANOVA (Pillai's trace: $V = 0.3$, $F(6, 62) = 1.82$, $p > 0.1$).

Myelin stained tissue sections showed an increase in the quantified staining intensity after the age of three weeks (Fig. 5). Further, a clear radial increase of staining intensity was noted from cortex surface

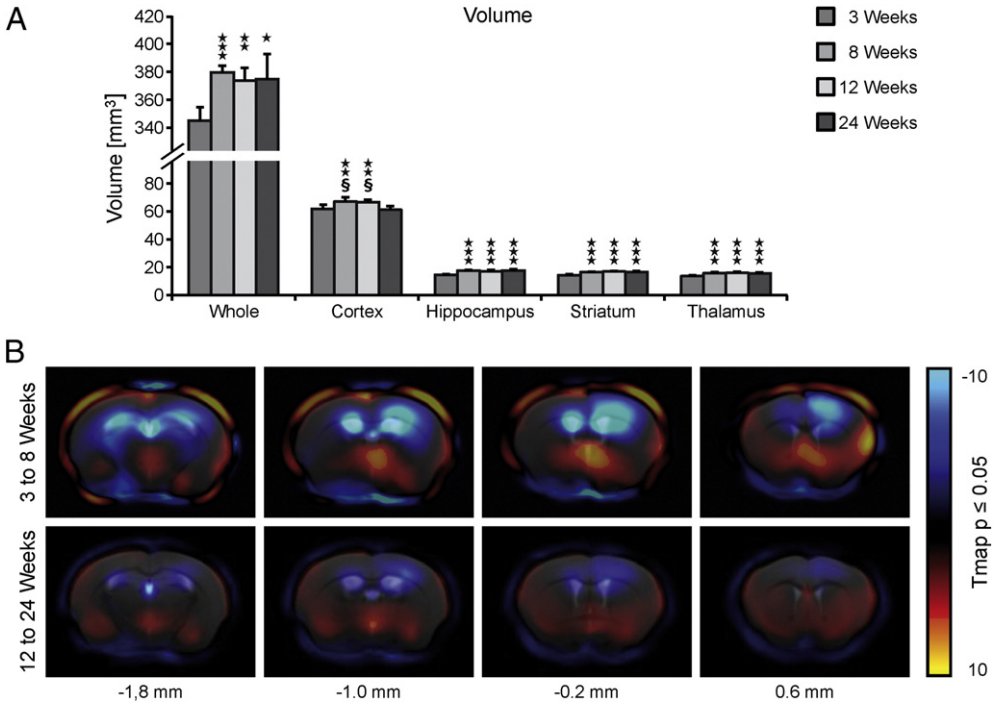

Fig. 2. Volume changes. Two different approaches to determine volume changes are shown here: ROI analysis (A) and deformation based morphometry (B). A: The mean volume of the different age groups is given for whole brain (as defined from cerebellum to olfactory bulb), cortex, hippocampus, striatum and thalamus (all four as defined by the ROIs in Inline Supplementary Fig. S1). Error bars show the standard error of the mean (SEM), significance levels are given corresponding to Fig. 1, here: difference to three weeks ($p < 0.05$ *; $p < 0.01$ **; $p < 0.001$ ***). B: T-maps superimposed onto the template brain. The T-maps depict the volume changes that are found significant in a t-test (with a p-value < 0.05) from three to eight weeks (upper row) and from twelve to twenty-four weeks (lower row). The T-values are color coded, with blue shades indicating a shrinkage in tissue and red shades representing a tissue expansion between the ages. Below, the position of the selected sections is given, relative to bregma.

towards the corpus callosum, independent of age group. ROIs corresponding to the cortical sections defined in the in vivo MRI were used to estimate the myelination intensity in these cortical sections as a function of age. This analysis revealed an effect of age for all three cortical sections (Pillai's trace: $V = 1.9$ $F(6,4) = 18.24$ $p < 0.01$). After three and again after eight weeks, the myelin content of the cortical layers increased substantially across all cortical layers. This observation holds for both S1 and M1.

Discussion

We have investigated the anatomic changes of the mouse brain during the first six months of age with the aim to discern developmental and maturation phases, thus identifying criteria of adult mouse brain. As we had reported in an earlier study on rat brain, maturation to a steady state "adult" situation of the brain takes much longer than sexual maturation. This distinction between developing/adolescent and adult brain is even more important in mice as they have become the most widely used species for a broad range of neuroscientific and neurological investigations, partly due to the easy access to transgenic animals. We realize that there are many aspects and corresponding variables to shape a complex picture of maturation. Among others there are neurotransmitter levels, receptor expressions or other molecular and cellular factors to be considered in further studies. Here, we have analyzed volume changes and structural alterations of the mouse brain using in vivo MRI. The use of different MRI modalities at high spatial resolution in combination with sophisticated image processing techniques make our approach sensitive for global and regional tissue growths, changes in laminar patterns and myelination in white and gray matter.

MRI parameter patterns of brain maturation

The combination of T2 and DTI contrasts has proven in the past to be highly sensitive for late developmental changes in the brain (Mengler et al., 2014). With increasing myelination and tightening of the myelin sheaths, T2 has been reported to decrease rapidly during the early postnatal phase, in rats as long as postnatal week eight (Wozniak and Lim, 2006). The T2 relaxation time continuously decreases from three weeks to twelve weeks, as observed in the present study, and is in agreement with earlier reports on T2 decrease (Hüppi and Dubois, 2006; Mengler et al., 2014; Samorajski and Rosten, 1973), caused predominantly by a reduction of tissue water content — further confirmed by decreasing proton density (Fig. 1) — and tissue reorganization processes. The increase of T2 between twelve and 24 weeks of age may indicate further late reorganization processes in the various anatomical ROIs (cf. Fig. 1) while in the case of the whole brain (Fig. 1) this only reflects the growing relative amount of free liquid in larger ventricles. Myelination and increasing cell density also contribute to the decrease

Fig. 3. Cortical thickness. A: the upper panel shows a lateral view onto the mouse brain, with the mean cortical thickness color coded on the surface, from left to right: three, eight, twelve and twenty-four weeks. The white line depicts the lateral thickness profile plotted in the diagram beneath. The mean cortical thickness is plotted from anterior to posterior for each of the four ages: three weeks (blue), eight weeks (red), twelve weeks (green), and twenty-four weeks (purple). B: mean cortical thickness from the anterior to posterior aspect of M1 and S1, respectively. The profile plotted, is showcased in the upper right corner of each graph. Instead of the standard deviation, the individual cortical thickness plots for M1 are illustrated in Supplementary Fig. 3 (Inline Supplementary Fig. S3).

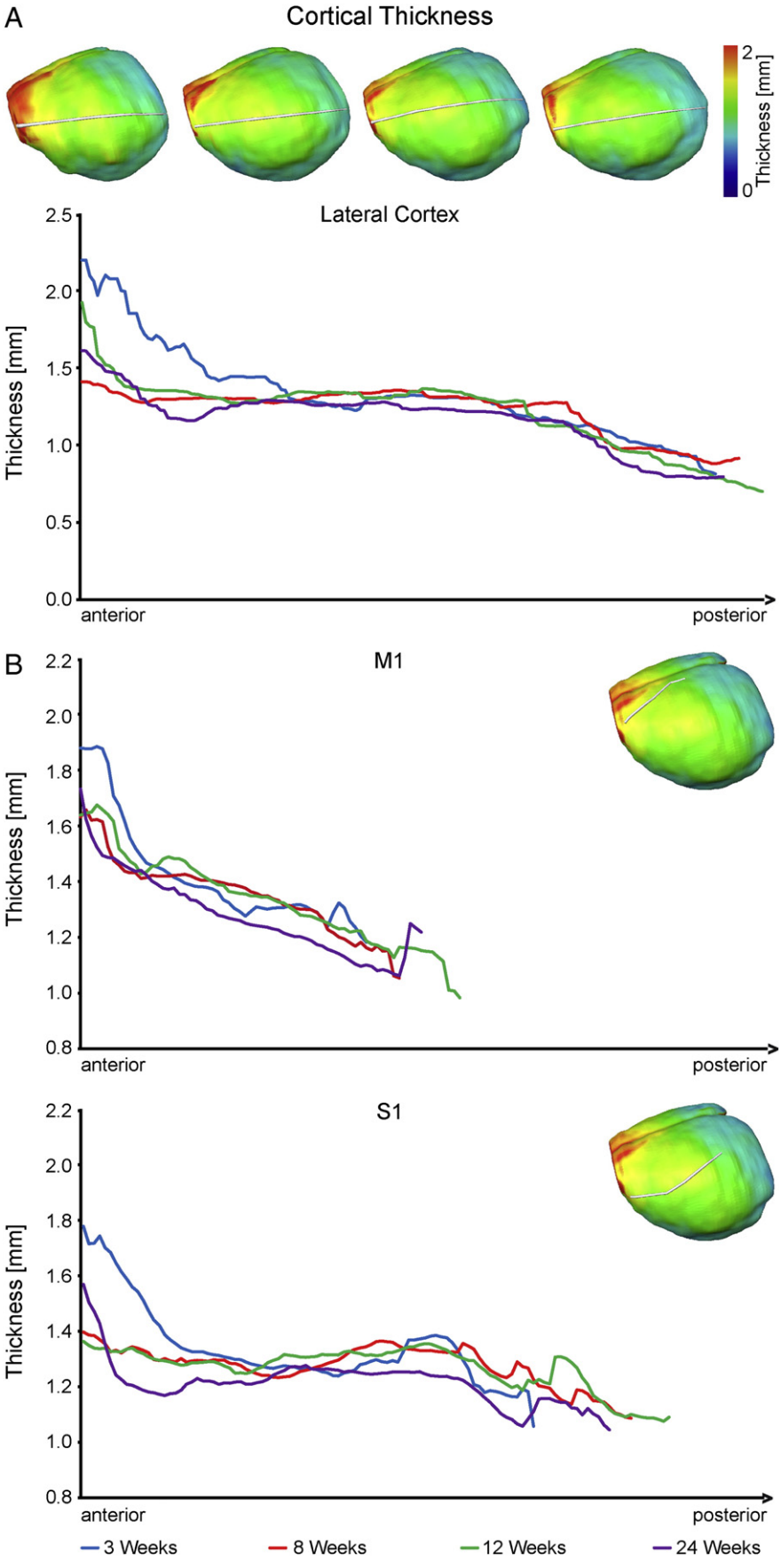
A
Cortical Thickness
2
0
Thickness [mm]
Lateral Cortex
Thickness [mm]
2.5
2.0
1.5
1.0
0.5
0.0
anterior
posterior
B
M1
Thickness [mm]
2.2
2.0
1.8
1.6
1.4
1.2
1.0
0.8
anterior
posterior
S1
Thickness [mm]
2.2
2.0
1.8
1.6
1.4
1.2
1.0
0.8
anterior
posterior
3 Weeks
8 Weeks
12 Weeks
24 Weeks

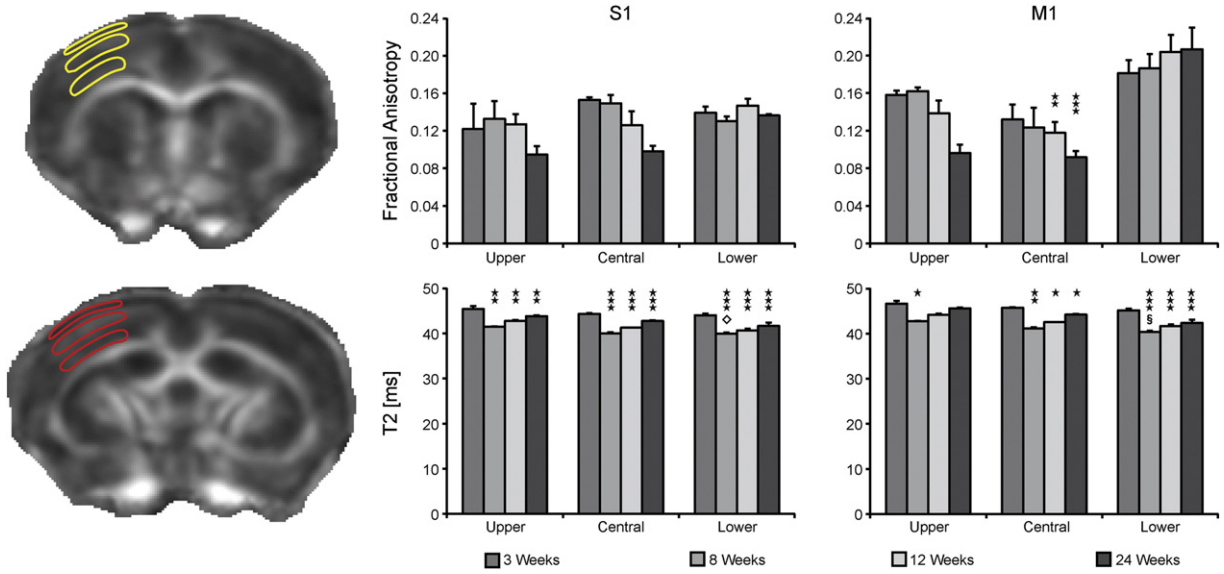

Fig. 4. MRI parameters in cortex layers. Left: FA maps of an eight week old mouse, superimposed with layer ROIs. For the sake of visibility, the ROIs do not represent the S1 or M1 ROIs but showcase the tangential position of the ROIs and their boundaries. Right: graphs show mean T2 and fractional anisotropy (FA) in S1 and M1 for the different age groups in the upper, central and lower cortex ROIs, as defined in the left panel. Error bars and significance levels are corresponding to Fig. 1.

of free water in the brain (Anderson et al., 2000; Chabert and Scifo, 2007) thus influencing T2 relaxation, as discussed in details in our earlier study on rat brain maturation (Mengler et al., 2014).

Myelination changes are well reflected in diffusion tensor parameters (Mengler et al., 2014). As the axial diffusivity values are not changing over age for most anatomical ROIs in our results, changes of fractional anisotropy (FA) are due to changes in radial diffusivity values. Although our present findings are different from results on dysmyelination in the shiverer mouse (Tyszka et al., 2006), they are conclusive and in line with earlier reports on FA and RD development (Deo et al., 2006; Mengler et al., 2014; Song et al., 2002). FA therefore can be used as surrogate reflecting the preferential orientation of myelin structures in a tissue volume. In most white matter ROIs (all except fimbrium), FA continuously increased in agreement with growing intensity on the Black and Gold II staining of myelin (Fig. 5). Gray matter ROIs show a slight decrease of FA with age indicating that ongoing tissue organization processes of network formation in gray matter reduce structural preferential orientations with time. Of all gray matter ROIs, this effect is most pronounced in the cortex (Fig. 1), continuing still between twelve and 24 weeks.

Cortical changes during maturation

The histological staining clearly shows for the cortex a layer-dependent and region dependent pattern that must be distinguished in the discussion of age dependent myelination. In an earlier study, Sizonenko et al. (2007) had divided the cortex into upper and lower cortex regions and reported a drop in FA and an initial drop in T2 followed by a gradual increase. Here, we subdivided the sensorimotor cortex into upper, middle and lower cortex sections, thus adding more detail to the region-specific evaluation. The upper two of the three sections overlaid on the cortex in the MRI images show a continuous decrease of FA with age. The lowest section is closely age independent in the somatosensory cortex area (S1) but is continuously increasing in the motor cortex (M1) (Fig. 4). While myelin staining shows an increasing staining intensity, FA decrease reflects the fact that the predominant radial cortical structure is increasingly challenged by growing horizontal layer organizations. The latter development results in reduction of preferential direction organization of diffusion. The different behaviors of the lowest section in the somatosensory and motor cortices, respectively, indicate that different time lines must be considered for this structural reorganization process in different anatomical cortex regions. A corresponding behavior is documented for barrel cortex and secondary somatosensory cortex (S2) in the supplement (Inline Supplementary Fig. S2). Furthermore, it shows the necessity to subdivide the cortex in layers for MRI analysis so that layer-dependent changes are not averaged out (Fig. 4 and Inline Supplementary Fig. S2) (Baloch et al., 2009). Summarizing these observations, the interlaminar differences in myelination, observed with histology, are matched by a radial gradient in T2 and FA values at the approximate position of the histological central layers II/III and lower layers IV–V. While quite low but stable with time in layers IV–VI, directionality decreases over time in layer II/III. As interlayer connections get stronger and myelination increases, the radial organization is superposed and the tangential layers of the neocortex are revealed.

The cortex volume changes only marginally over the period three to 24 weeks, in contrast to the situation in rats where cortical volume kept increasing during the first three months (Mengler et al., 2014). Cortical thickness in rats increases during the first month, but then stagnates. In mice, we have observed a gradual cortex thickness decrease from rostral to caudal (Fig. 3), independent of age. With growing age, this thickness is decreasing in all positions along the rostral–caudal line, but this age dependent decrease is most pronounced at the rostral end. In general, there is a global tendency to level out this thickness gradient along the rostral–caudal line with increasing age. Thus, the cortex volume of mice remains closely constant from three weeks as the continuing thickness decrease compensates for the brain volume increase with age. In rats, the continuing cortex volume increase is explained by brain expansion paralleled by thickness stabilization after four weeks of age.

Consequences for age determination of a fully matured mouse brain

From the present findings, it becomes clear that one needs to carefully choose the desired variable to define a stable condition, which is no longer varied by increasing age. Cortex volume appears not to be a sensitive parameter, while cortical thickness is more suitable: the most drastic decrease occurs during the first eight to twelve weeks, after which time only slight changes are noted. Also, the MRI parameters, T2 and FA, generally show their most pronounced changes during

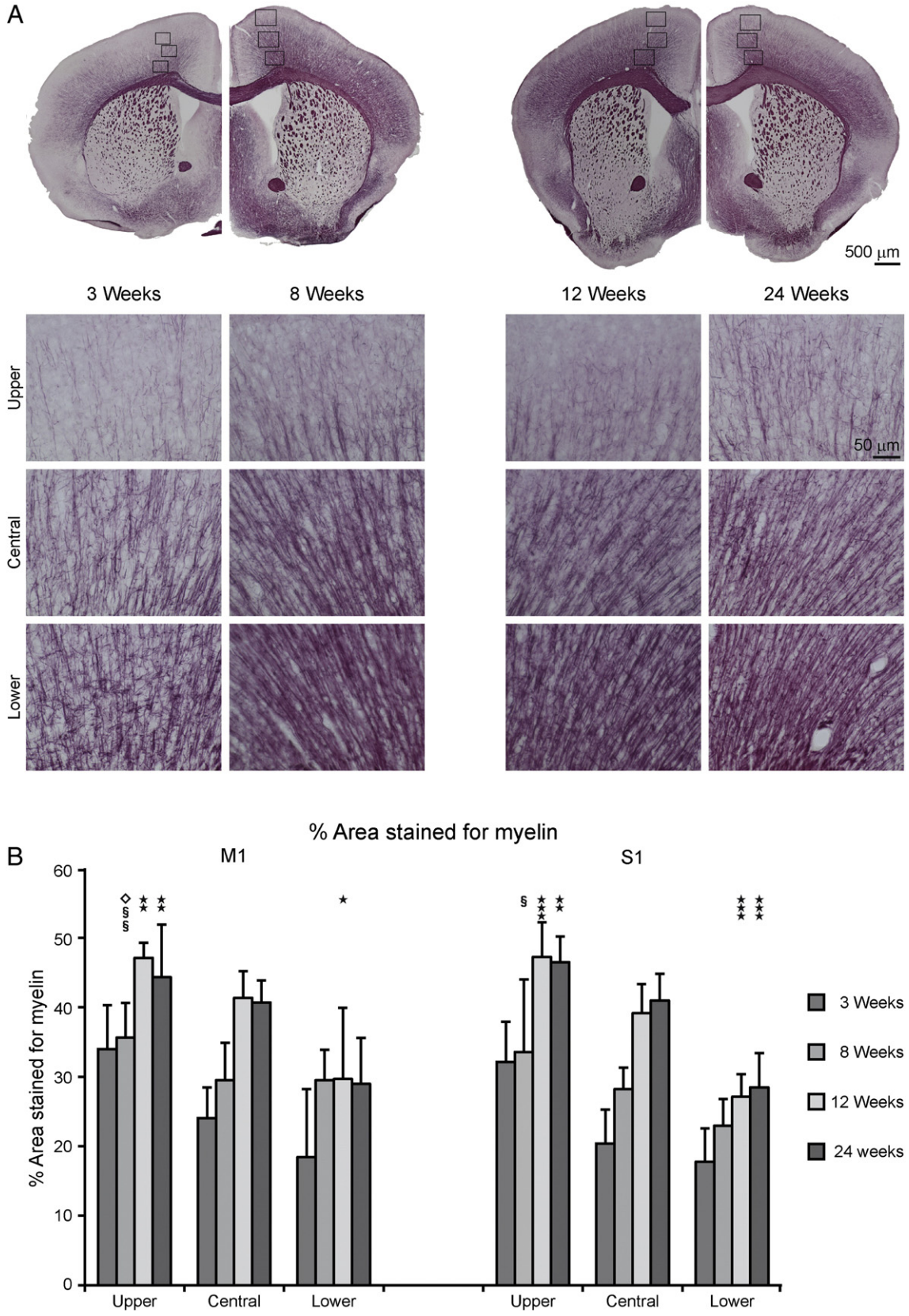

Fig. 5. Myelin content in cortex layers. A: representative myelin staining from a three, eight, twelve and twenty-four week old mouse. The upper row shows an overview of one hemisphere (4× magnification) for every age. Close-ups from the indicated positions were taken with 40× magnification in the upper, central and lower cortices. Shown here are ROIs in M1. B: quantification of myelin content in upper, central and lower M1 and S1, given by the percentage of myelin stained area. Error bars and significance levels are corresponding to Fig. 1.

the first two to three months. When using myelination as maturation criteria, very pronounced increases were observed till twelve weeks of age, with only minor changes thereafter.

Taken these different criteria together, it appears best to define the period up to month three as adolescent with clear maturation dependent alterations. From three months of age, with only very small further changes observed, beginning adulthood of the mouse brain may be considered. This distinction is of importance as many studies on cerebral diseases are based on the assumption of dealing with adult animals as analysis of disease development should not be modulated by ongoing maturation processes. From our present results, it appears advisable to prefer mice of three months of age or even older when stable, adult brains as baseline must be demanded.

Conclusions

We have followed various anatomic changes and tissue characterization by MRI parameters as well as myelination as a function of brain age in the mouse. Our results clearly indicate that the adolescent phase with ongoing changes in the brain lasts at least till three months of age. For the large number of studies involving mouse brains for genetic investigations with transgenic animals or for neurological disease studies, mice should be used at the age of three months or later when adult animals are required. However, it must be cautioned that our various applied metrics show different behaviors with some reaching stabilization earlier than others. Thus, the relevance of the chosen metric in future studies will influence the choice of age window for stable brain conditions.

Acknowledgments

We thank Melanie Nelles and Michael Diedenhofen from the Max Planck Institute for Metabolism Research for technical support and Ulla Uhlenküken for the professional preparation of figures. This research was supported by grants from the FP7 European Union program TargetBraIn (LH: HEALTH-F2-2012-279017), BrainPath (AK; MH: PIAPP-GA-2013-612360), and GlowBrain (SS: REGPOT-2012-CT2012-316120).

References

Adamczak, J., Schneider, G., Nelles, M., Que, I., Suidgeest, E., van der Weerd, L., Löwik, C., Hoehn, M., 2014. In vivo bioluminescence imaging of vascular remodeling after stroke. Front. Cell. Neurosci. 8 (Article 274).

Andersen, S.L., 2003. Trajectories of brain development: point of vulnerability or window of opportunity? Neurosci. Biobehav. Rev. 27, 3–18.

Anderson, A.W., Xie, J., Pizzonia, J., Bronen, R.A., Spencer, D.D., Gore, J.C., 2000. Effects of cell volume fraction changes on apparent diffusion in human cells. Magn. Reson. Imaging 18, 689–695.

Baloch, S., Verma, R., Huang, H., Khurd, P., Clark, S., Yarowsky, P., Abel, T., Mori, S., Davatzikos, C., 2009. Quantification of brain maturation and growth patterns in C57BL/6J mice via computational neuroanatomy of diffusion tensor images. Cereb. Cortex 19, 675–687.

Basser, P.J., Mattiello, J., Lebihan, D., 1994. Estimation of the effective self-diffusion tensor from the NMR spin-echo. J. Magn. Reson. Ser. B 103, 247–254.

Bockhorst, K.H., Narayana, P.A., Liu, R., Vijjula, P.A., Ramu, J., Kamel, M., Wosik, J., Bockhorst, T., Hahn, K., Hasan, K.M., Perez-Polo, J.R., 2008. Early postnatal development of rat brain: in vivo diffusion tensor imaging. J. Neurosci. Res. 86, 1520–1528.

Chabert, S., Scifo, P., 2007. Diffusion signal in magnetic resonance imaging: origin and interpretation in neurosciences. Biol. Res. 40, 385–400.

Deo, A.A., Grill, R.J., Hasan, K.M., Narayama, P.A., 2006. In vivo serial diffusion tensor imaging of experimental spinal cord injury. J. Neurosci. Res. 83, 801–810.

Franklin, K.B.L.P.G. (Ed.), 2007. The Mouse Brain in Stereotaxic Coordinates, 3rd ed. Elsevier Academic Press, San Diego, CA.

Hüppi, P.S., Dubois, J., 2006. Diffusion tensor imaging of brain development. Semin. Fetal Neonatal Med. 11, 489–497.

Jones, D.K., Horsfield, M.A., Simmons, A., 1999. Optimal strategies for measuring diffusion in anisotropic systems by magnetic resonance imaging. Magn. Reson. Med. 42, 515–525.

Khmelinskii, A., Mengler, L., Kitslaar, P., Staring, M., Hoehn, M., Lelieveldt, B.P.F., 2013. A visualization platform for high-throughput, follow-up, co-registered multi-contrast MRI rat brain data. Medical Imaging 2013: Biomedical Applications in Molecular, Structural, and Functional Imagingp. 8672.

Klein, S., Staring, M., Murphy, K., Viergever, M.A., Pluim, J.P.W., 2010. elastix: a toolbox for intensity-based medical image registration. IEEE Trans. Med. Imaging 29, 196–205.

Leow, A.D., Klunder, A.D., Jack, C.R., Toga, A.W., Dale, A.M., Bernstein, M.A., Britson, P.J., Gunter, J.L., Ward, C.P., Whitwell, J.L., Borowski, B.J., Fleisher, A.S., Fox, N.C., Harvey, D., Kornak, J., Schuff, N., Studholme, C., Alexander, G.E., Weiner, M.W., Thompson, P.M., 2006. Longitudinal stability of MRI for mapping brain change using tensor-based morphometry. NeuroImage 31, 627–640.

Meaney, M.J., Stewart, J., 1981. A descriptive study of social development in the rat (*Rattus norvegicus*). Anim. Behav. 29, 34–45.

Mengler, L., Khmelinskii, A., Diedenhofen, M., Po, C., Staring, M., Lelieveldt, B.P., Hoehn, M., 2014. Brain maturation of the adolescent rat cortex and striatum: changes in volume and myelination. NeuroImage 84, 35–44.

Mori, S., Itoh, R., Zhang, J.Y., Kaufmann, W.E., van Zijl, P.C.M., Solaiyappan, M., Yarowsky, P., 2001. Diffusion tensor imaging of the developing mouse brain. Magn. Reson. Med. 46, 18–23.

Paxinos, G., Franklin, K.B., 2001. The Mouse Brain in Stereotaxic Coordinates. Academic Press.

Samorajski, T., Rosten, C., 1973. Age and regional differences in the chemical composition of brains of mice, monkeys and humans. Progress in Brain Research: Neurobiological Aspects of Maturation and Aging. Elsevier, pp. 253–265.

Schmued, L., Bowyer, J., Cozart, M., Heard, D., Binienda, Z., Paule, M., 2008. Introducing Black-Gold II, a highly soluble gold phosphate complex with several unique advantages for the histochemical localization of myelin. Brain Res. 1229, 210–217.

Sizonenko, S.P.V., Camm, E.J., Garbow, J.R., Maier, S.E., Inder, T.E., Williams, C.E., Neil, J.J., Huppi, P.S., 2007. Developmental changes and injury induced disruption of the radial organization of the cortex in the immature rat brain revealed by in vivo diffusion tensor MRI. Cereb. Cortex 17, 2609–2617.

Skare, S., Hedehus, M., Moseley, M.E., Li, T.Q., 2000. Condition number as a measure of noise performance of diffusion tensor data acquisition schemes with MRI. J. Magn. Reson. 147, 340–352.

Smith, S.M., 2002. Fast robust automated brain extraction. Hum. Brain Mapp. 17, 143–155.

Song, S.K., Sun, S.W., Ramsbottom, M.J., Chang, C., Russell, J., Cross, A.H., 2002. Dysmyelination revealed through MRI as increased radial (but unchanged axial) diffusion of water. NeuroImage 17, 1429–1436.

Spear, L.P., Brake, S.C., 1983. Periadolescence: age-dependent behavior and psychopharmacological responsivity in rats. Dev. Psychobiol. 16, 83–109.

Tissir, F., Goffinet, A.M., 2003. Reelin and brain development. Nat. Rev. Neurosci. 4, 496–505.

Tyszka, J.M., Readhead, C., Bearer, E.L., Pautler, R.G., Jacobs, R.E., 2006. Statistical diffusion tensor histology reveals regional dysmyelination effects in the shiverer mouse mutant. NeuroImage 29, 1058–1065.

van Dorsten, F.A., Hata, R., Maeda, K., Franke, C., Eis, M., Hossmann, K.-A., Hoehn, M., 1999. Diffusion- and perfusion-weighted MR imaging of transient focal cerebral ischaemia in mice. NMR Biomed. 12, 525–534.

Webster, S.J., Van Eldik, L.J., Watterson, D.M., Bachstetter, A.D., 2015. Closed head injury in an age-related Alzheimer mouse model leads to an altered neuroinflammatory response and persistent cognitive impairment. J. Neurosci. 35, 6554–6569.

Wozniak, J.R., Lim, K.O., 2006. Advances in white matter imaging: a review of in vivo magnetic resonance methodologies and their applicability to the study of development and aging. Neurosci. Biobehav. Rev. 30, 762–774.

Yanovsky, I., Thompson, P.M., Osher, S., Leow, A.D., 2008. Asymmetric and symmetric unbiased image registration: statistical assessment of performance. 2008 IEEE Computer Society Conference on Computer Vision and Pattern Recognition Workshops, pp. 1–3.

Zempel, H., Mandelkow, E., 2014. Lost after translation: missorting of tau protein and consequences for Alzheimer disease. Trends Neurosci. 37, 721–732.

Zhang, J.Y., Richards, L.J., Yarowsky, P., Huang, H., van Zijl, P.C.M., Mori, S., 2003. Three-dimensional anatomical characterization of the developing mouse brain by diffusion tensor microimaging. NeuroImage 20, 1639–1648.

Zhang, J.Y., Miller, M.I., Plachez, C., Richards, L.J., Yarowsky, P., van Zijl, P., Mori, S., 2005. Mapping postnatal mouse brain development with diffusion tensor microimaging. NeuroImage 26, 1042–1051.